Article:

Krynkin, A. orcid.org/0000-0002-8495-691X, Horoshenkov, K.V. and Van Renterghem, T. (2016) An airborne acoustic method to reconstruct a dynamically rough flow surface. Journal of the Acoustical Society of America, 140 (3). pp. 2064-2073. ISSN 0001-4966

https://doi.org/10.1121/1.4962559

An airborne acoustic method to reconstruct a dynamically rough flow surface

Anton Krynkin[1], Kirill V. Horoshenkov
Department of Mechanical Engineering, University of Sheffield,
Sheffield, S1 3JD, UK

Timothy Van Renterghem
Department of Information Technology, Ghent University, St.-Pietersnieuwstraat
41, 9000 Gent, Belgium

[1]e-mail: a.krynkin@sheffield.ac.uk

Abstract

Currently, there is no airborne in-situ method to reconstruct with high fidelity the instantaneous elevation of a dynamically rough surface of a turbulent flow. This work proposes a new holographic method that reconstructs the elevation of a 1-D rough water surface from airborne acoustic pressure data. This method can be implemented practically using an array of microphones deployed over a dynamically rough surface or using a single microphone which is traversed above the surface at a speed that is much higher than the phase velocity of the roughness pattern. In this work, the theory is validated using synthetic data calculated with the Kirchhoff approximation and a finite difference, time domain method over a number of measured surface roughness patterns. The proposed method is able to reconstruct the surface elevation with a sub-millimetre accuracy and over a representatively large area of the surface. Since it has been previously shown that the surface roughness pattern reflects accurately the underlying hydraulic processes in open channel flow (e.g. [Horoshenkov, et al, J. Geoph. Res.,118(3), 18641876 (2013)]), the proposed method paves the way for the development of new non-invasive instrumentation for flow mapping and characterization that are based on the acoustic holography principle.

PACS: 43.20.Ye, 43.30.Hw, 43.28.Gq

Keywords: Acoustic scattering, roughness, dynamic surface, inverse method

I Introduction

Understanding the spatial and temporal hydraulic changes in rivers and other types of open channels is of paramount importance for predicting flood risk, sediment movement and consequent morphological change. Understanding the spatial and temporal variability of flows has become a core element in assessing the water quality and ecological status of rivers (EU Water Framework Directive (WFD)). However, there is a significant shortcoming in our ability to monitor these flows at sufficient temporal and spatial resolution particularly during extreme events because there is no technology that can be deployed rapidly to accurately map the hydraulic and topographical information of rivers at a reach scale. Although attempts have been made to measure the dynamic surface roughness pattern underwater (e.g. [1, 2]), there is still a lack of real time airborne methods to measure the instantaneous surface elevation with sub-millimeter accuracy and at a very high temporal resolution. This information is of great importance for us to advance the existing theoretical link between the free surface behaviour and the underlying turbulent flow structures which carry information about the flow and sediment bed [3]. This link can be used to study the changes in the turbulent flow structures and velocity depth profile remotely for a range of open channel flows in the laboratory and in the field using an array of acoustic sensors deployed on a large scale, e.g. with a swarm of unmanned aerial vehicles (UAV).

The main focus of this paper is to present a new method based on acoustic boundary integral equations and a pseudo-inverse technique applied to a matrix based equation to recover the instantaneous elevation of a dynamically rough surface at sub-millimeter accuracy, high temporal resolution and a representatively large spatial scale. In particular, this approach enables us to study the acoustic scattering from an inhomogeneous roughness that supports multiple scales.

The paper is organized in the following manner. Section II presents the underlying theory of acoustic scattering. This theory is then used in combination with the matrix inversion method which is described in Section III. Section IV presents the results of the application of the proposed inversion method to the acoustic pressure data which were predicted with the standard Kirchhoff approximation and with the Finite Difference Time Domain (FDTD) method. The conclusions are drawn in Section V.

II Scattering of acoustic waves from a rough surface

Let us consider a semi-infinite space in Cartesian coordinate system $Oxyz$ bounded by rough surface S which mean plane S_0 coincide with Oxy coordinate plane. Spatial scales and distribution of surface elevation $\zeta(x)$ are assumed to be arbitrary within the validity range of the proposed method and in this paper both deterministic and random profiles are tested. In order to simplify the numerical calculations, it is assumed that the surface is uniform in Oy-direction and the acoustic source is a directional line source which directivity pattern $A(x, z)$ is defined in Section IV. This makes the stated problem one dimensional. The main axis of the far-field directivity pattern is inclined at the angle ψ_0 with respect to the Ox axis and it is aligned with the centre of coordinates. The coordinates of the source and receiver are defined by (x_1, z_1) and (x_2, z_2), respectively. The source emits a continuous harmonic wave $\exp(-\mathrm{i}\omega t)$ with angular frequency ω and constant amplitude in time.

In this paper the roughness is defined by the dynamic behaviour of the water flow free surface. To maintain harmonic dependence on time, as suggested above, it is assumed that the roughness is frozen over a short time period at which the complex acoustic pressure of the scattered harmonic wave needs to be measured. This is true because the speed of sound in air $c_0 = 340$ m/s is much faster than the maximum phase velocity $U = U_0 + c_p$ at which the surface roughness pattern on the flow surface of a typical shallow water river with the mean depth h will propagate, i.e. $c_0 \gg U$. Here U_0 denotes the flow velocity and $c_p = \sqrt{gh}$ is the phase velocity of the gravity waves, g is the gravity.

In this paper the scattering from a rough surface is approximated by the tangent plane approximation as suggested in [4]. We assume that the surface is rigid which is a good approximation for the case when sound propagates in air above a dynamically rough water surface, e.g. free surface of a turbulent open channel flow. The approximation is based on the Kirchhoff method and principles of geometrical optics (e.g. [5]), and it is valid if local curvature radius a of the rough surface is much greater than the acoustic wavelength $\lambda = 2\pi/k$, where k is wavenumber of the acoustic wave. For the diffraction on a sphere, this condition can be stated in the following form

$$\sin\psi \gg \frac{1}{(ka)^{1/3}}, \tag{1}$$

where a is a radius of the sphere locally inscribed in rough surface. The condition in eq. (1) can be relaxed to [6]

$$\sin\psi > \frac{1}{(ka)^{1/3}}, \tag{2}$$

so that the Kirchhoff approach remains accurate for the incident angles far from the low grazing angles. In this paper condition (2) is used in the numerical simulation to define the surface.

Assuming that the distances from the source R_1 and receiver R_2 to a given point on the mean surface (see Figure 1) are much greater than the acoustic wavelength

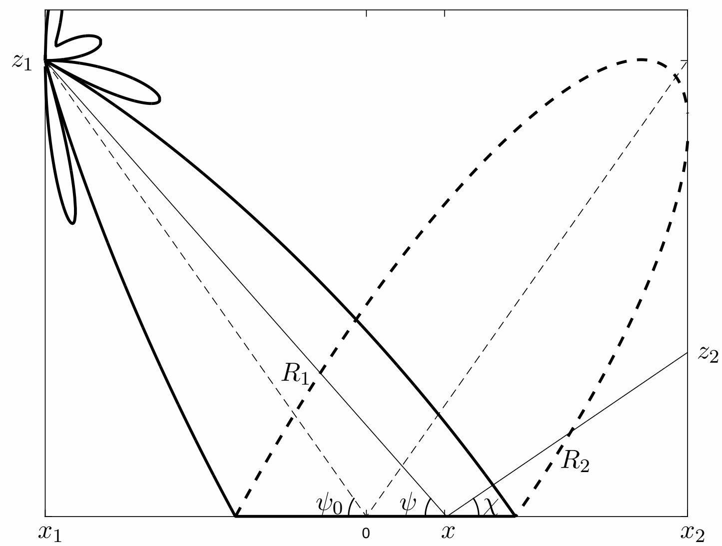

Figure 1: The geometry of the acoustic problem of rough surface scattering.

and using the Kirchhoff method, the scattered acoustic pressure can be approximated by [4, 7]

$$p(x_2, z_2) = -\frac{\mathrm{i}}{2\pi k} \int_{S_0} \frac{A(x)}{\sqrt{R_1 R_2}} \exp\left[\mathrm{i}k(R_1 + R_2) - \mathrm{i}q_z \zeta(x)\right] \left[q_z - q\frac{\partial \zeta(x)}{\partial x}\right] dx, \quad (3)$$

where $\zeta(x)$ is surface elevation and

$$q_z = k\left(\frac{z_1}{R_1} + \frac{z_2}{R_2}\right), \quad (4)$$

$$q = -k\left(\frac{x_1 - x}{R_1} + \frac{x_2 - x}{R_2}\right), \quad (5)$$

$$R_1 = \sqrt{(x - x_1)^2 + z_1^2}, \quad (6)$$

$$R_2 = \sqrt{(x - x_2)^2 + z_2^2}. \quad (7)$$

Assuming that the surface is smooth, $\partial\zeta(x)/\partial x \ll 1$, equation (3) can be simplified to

$$p(x_2, z_2) = -\frac{\mathrm{i}}{2\pi k}\int_{S_0} \frac{A(x)}{\sqrt{R_1 R_2}} \exp\left[\mathrm{i}k(R_1 + R_2) - \mathrm{i}q_z\zeta(x)\right] q_z dx. \quad (8)$$

If the profile of the surface $\zeta(x)$ is known than the integral in equation (8) can be solved numerically. However, the surface in the above integral is assumed to be unknown and it is the acoustic pressure in the left hand side which is known from experiments or from synthetic data (obtained with the Kirchhoff approximation and FDTD method in this paper). This formulates an inversion problem where the variable $\zeta(x)$ needs to be recovered from the available acoustic pressure data.

III Matrix inverse method

In order to invert the surface elevation $\zeta(x)$ it is proposed to use a numerical approach to solve integral equation (8). For this purpose the integral is discretised over the surface S_0 with the M uniform spatial elements $\Delta x = x_{m+1} - x_m$, $m = 1, ..., M$ and approximated by the sum over these elements. It is noted that the size of the element Δx has to be at least five times smaller than the acoustic wavelength λ[6] (i.e. $\Delta x < \lambda/5$). The scattered acoustic pressure at the receiver position (x_2, z_2) can be approximated by

$$p(x_2, z_2) = -\frac{\mathrm{i}}{2\pi k}\sum_{m=1}^{M} \frac{A(x_m)}{\sqrt{R_{1,m} R_{2,m}}} \exp\left[\mathrm{i}k(R_{1,m} + R_{2,m}) - iq_{z,m}\zeta(x_m)\right] q_{z,m}\Delta x, \quad (9)$$

where all the terms with the index m are defined at points x_m, $m = 1, ..., M$ on the surface S_0. Equation (9) can be rewritten in the form of a scalar product of two vectors

$$p(x_2, z_2) = \boldsymbol{D}_M \boldsymbol{E}_M, \quad (10)$$

where

$$\boldsymbol{D}_M = \left\{ -\frac{\mathrm{i}}{2\pi k} \frac{A(x_m)}{\sqrt{R_{1,m}R_{2,m}}} \exp\left[\mathrm{i}k(R_{1,m} + R_{2,m})\right] q_{z,m}\Delta x \right\}_{m=1,...,M}, \tag{11}$$

$$\boldsymbol{E}_M = \left\{\exp\left[-\mathrm{i}q_{z,m}\zeta(x_m)\right]\right\}_{m=1,...,M}. \tag{12}$$

In order to retrieve the surface profile $\zeta(x)$ it is necessary to have acoustic pressure data recorded at more than one receiver positions that the acoustic pressure vector $\boldsymbol{P}$ with N elements can be formed. With multiple receiver positions defined by the coordinates $(x_{2,n}, z_{2,n})$, $n = 1, ..., N$, equation (10) needs to be converted into the matrix form in order to apply the matrix inversion.

One way of deriving the matrix form is to isolate the unknown elevation of the rough surface $\zeta(x)$ at the points x_m, $m = 1, ..., M$ for all receiver positions in one single vector $\boldsymbol{E}_M$. In doing so it is assumed that for fixed index m the variability of $q_{z,mn}$, $n = 1..N$ with respect to the position on the surface is negligible in the vicinity of the specular point defined by the angle ψ_0 as shown in Figure 1. This gives

$$\boldsymbol{P}_{N\times 1} = \boldsymbol{H}_{N\times M}\boldsymbol{E}_{M\times 1}, \tag{13}$$

where the elements of the matrix $\boldsymbol{H}_{N\times M}$ are defined by

$$h_{mn} = \left\{ -\frac{\mathrm{i}}{2\pi k} \frac{A(x_{mn})}{\sqrt{R_{1,mn}R_{2,mn}}} \exp\left[\mathrm{i}k(R_{1,mn} + R_{2,mn})\right] q_{z,mn}\Delta x \right\}_{m=1,...,M,n=1,...,N} \tag{14}$$

and unknown vector $\boldsymbol{E}_{M\times 1}$ is given by equation (12) with $q_{z,m}$ defined by the receiver positioned at the specular angle ψ_0. The form of equation (13) is identical to that used in inverse frequency response function (IFRF) techniques with $\boldsymbol{H}_{N\times M}$ representing transfer matrix for an array of microphones and vector $\boldsymbol{E}_{M\times 1}$ representing velocity potentials on the surface [11]. This allows us to apply previously developed techniques to recover surface profile.

It is practical to assume that the number M of unknown points on the surface is greater than the number of receivers N ($M > N$). However, this leads to an under-determined system of equations which may result in an ill-conditioned matrix and a non-unique inverse solution to problem stated in equation (13). In order to invert the matrix $\boldsymbol{H}_{N\times M}$ in equation (13) it is proposed to use a pseudo-inverse method based on the singular value decomposition technique (SVD) (e.g. [8]). Applied to matrix $\boldsymbol{H}_{N\times M}$ this gives

$$\boldsymbol{H}_{N\times M} = \boldsymbol{U}_{N\times N}\boldsymbol{S}_{N\times M}\bar{\boldsymbol{V}}^{T}_{M\times M}, \tag{15}$$

where $\boldsymbol{U}_{N\times N}$ and $\boldsymbol{V}_{M\times M}$ are unitary matrices (defined by $\boldsymbol{A}\bar{\boldsymbol{A}}^{T} = \boldsymbol{I}$), $\boldsymbol{S}_{N\times M}$ is a diagonal matrix with nonnegative elements arranged in the descending order of smallness, $\bar{\mathbf{A}}$ stands for complex conjugate and $\mathbf{A}^{T}$ denotes matrix transpose. In order to apply pseudo-inverse techniques and decrease the computational time, in this paper the truncated form of matrices $\boldsymbol{S}$ and $\boldsymbol{V}$ in equation (15) was used so that

$$\boldsymbol{H}_{N\times M} = \boldsymbol{U}_{N\times N}\boldsymbol{S}_{N\times N}\bar{\boldsymbol{V}}^{T}_{N\times M}. \tag{16}$$

Applying the SVD to equation (13) and using the definition of the unitary matrix the unknown vector $\boldsymbol{E}_{M\times 1}$ can be expressed in the following form

$$\boldsymbol{E}_{M\times 1} = \boldsymbol{V}_{M\times N}\boldsymbol{S}^{-1}_{N\times N}\bar{\boldsymbol{U}}^{T}_{N\times N}\boldsymbol{P}_{N\times 1}, \tag{17}$$

where $\boldsymbol{S}^{-1}_{N\times N}$ indicates the matrix inverse. The matrix $\boldsymbol{S}_{N\times N}$ may contain small order elements resulting in singular values in the inverted matrix $\boldsymbol{S}^{-1}_{N\times N}$. In order to regularize ill-conditioned matrix and to filter the singular elements from the inverse matrix it is proposed to use the Tikhonov regularization technique (e.g. [11] and [9]) that gives

$$\boldsymbol{E}_{M\times 1} = \boldsymbol{V}_{M\times N}\boldsymbol{S}^{-1}_{\beta,N\times N}\bar{\boldsymbol{U}}^{T}_{N\times N}\boldsymbol{P}_{N\times 1}, \tag{18}$$

where $\boldsymbol{S}_{\beta,N\times N}^{-1} = \left[\boldsymbol{S}_{N\times N} + \beta^2 \boldsymbol{S}_{N\times N}^{-1}\right]^{-1}$ and β is the regularization parameter. In order to adjust parameter β we used the generalised cross validation (GCV) technique. This technique requires to minimize the following function

$$F(\beta) = \frac{r_\beta^2}{Tr\left(\boldsymbol{I}_{N\times N} - \boldsymbol{U}_{N\times N}\boldsymbol{S}_{N\times N}\boldsymbol{S}_{\beta,N\times N}^{-1}\bar{\boldsymbol{U}}_{N\times N}^{T}\right)^2}, \tag{19}$$

in which r_β is the residue defined by l^2-vector norm

$$r_\beta = \left|\left|\left(\boldsymbol{I}_{N\times N} - \boldsymbol{U}_{N\times N}\boldsymbol{S}_{N\times N}\boldsymbol{S}_{\beta,N\times N}^{-1}\bar{\boldsymbol{U}}_{N\times N}^{T}\right)\boldsymbol{P}_{N\times 1}\right|\right|. \tag{20}$$

The argument (phase) of each element of vector $\boldsymbol{E}_{M\times 1}$ provides information about the surface elevation. In order to retrieve the phase from matrix equation (18) the complex natural logarithm is applied element-wise to the results of the matrix product. This yields

$$\boldsymbol{Q}_{\boldsymbol{\zeta}_{M\times 1}} = -\Im[\mathrm{Ln}(\boldsymbol{E}_{M\times 1})], \tag{21}$$

where

$$\boldsymbol{Q}_{\boldsymbol{\zeta}_{M\times 1}} = \{q_{z,m}\zeta(x_m)\}_{m=1,\ldots,M}, \tag{22}$$

with $\Im(<\cdot>)$ representing the imaginary part of the natural logarithm. It is noted that the application of Ln in equation (21) is restricted to the case when $-\pi < q_{z,m}\zeta(x_m) < \pi$ that enables us to uniquely define the elements of the vector $\boldsymbol{Q}_{\boldsymbol{\zeta}_{M\times 1}}$. This condition holds in the vicinity of a specular point defined by the angle ψ_0 and fails as distance between specular point and x_m, $m = 1, ..., M$ increases. The discretized roughness profile $\{\zeta_m\}$ at the points $\{x_m\}$ can then be deduced as

$$\{\zeta_m\}_{m=1,\ldots,M} = \left\{\frac{-\Im[\mathrm{Ln}(e_m)]}{q_{z,m}}\right\}_{m=1,\ldots,M}, \tag{23}$$

where e_m is an element of the vector $\boldsymbol{E}_{M\times 1}$.

The fact that the proposed inversion largely depends on the proximity of a surface point to the specular point leads to the idea of replacing the directional source with simple monopole with a unit amplitude. As a result, the elements of the matrix $\boldsymbol{H}_{N\times M}$ can be simplified to

$$h_{mn} = \left\{ -\frac{\mathrm{i}}{2\pi k} \frac{\exp\left[\mathrm{i}k(R_{1,mn} + R_{2,mn})\right]}{\sqrt{R_{1,mn} R_{2,mn}}} q_{z,mn} \Delta x \right\}_{m=1,\dots,M, n=1,\dots,N}. \tag{24}$$

This reduces input data to geometrical parameters defined by the position of source and receivers with respect to the surface S_0 and data recorded on the array of receivers.

IV Results

In this paper, validation of the proposed inversion method (equation (23)) is based on two sets of synthetic data generated using the Kirchhoff integral and FDTD method. The former demonstrates the implementation of the proposed inverse technique and the latter shows application of this technique to independent set of data obtained in order to retrieve unknown surface profile.

A Simulated roughness

In this section the acoustic pressure scattered by the rough surface was modelled with the Kirchhoff integral (equation (8)). In order to reconstruct the surface elevation it was proposed to use an array of $N = 121$ receivers arranged on a circular arch with the radius of $R = 0.4$ m as illustrated in Figure 2. The receivers and source are positioned on the opposite sides of the arch. The arch is suspended at $d = 0.01$ m above the mean surface of water, S_0, and the centre of the arch coincides with the centre of

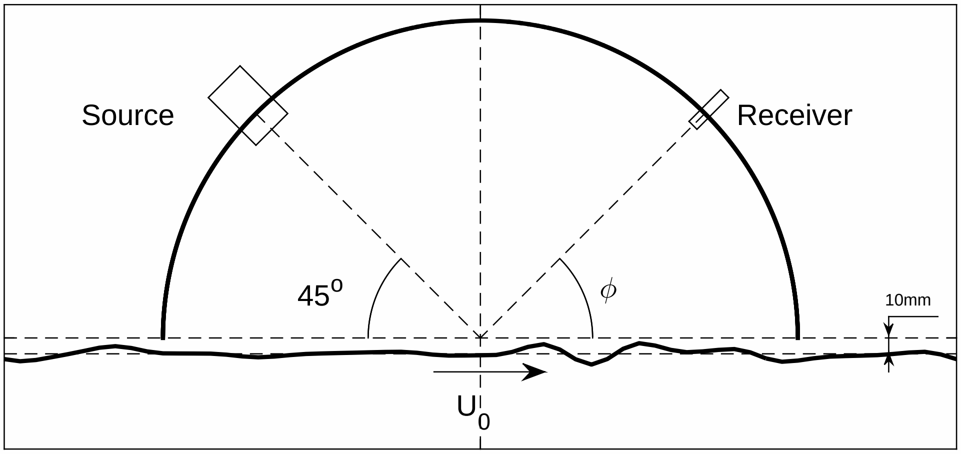

Figure 2: The acoustic setup used to reconstruct the rough surface in the numerical experiment.

Ox axis. The source was installed at the angle of $\psi_0 = 45^o$ and its coordinates were $(R\cos\psi_0, R\sin\psi_0 + d)$, where d is the vertical distance of the circular arch base to the plane S_0. The position of receivers is defined by $(-R\cos\phi, R\sin\phi + d)$, where ϕ varies from 15^o to 75^o with 0.5^o resolution that produces 121 receiver positions. The sound source emitted a continuous harmonic wave at $f = 43$ kHz and its far-field directivity pattern was defined by

$$A(\theta) = \frac{J_1(ka\sin\theta)}{ka\sin\theta}, \tag{25}$$

where $a = 0.02$ m is the radius of the source aperture. The position of the receivers was characterized by the angle ϕ which was taken from the horizontal line. The number of the receivers in the array, N, and the adopted geometry were consistent with that used in the experiments reported by Nichols [10]. Increasing the number of receivers may result in more singular values and it may lead to a more unstable inverse solution. Decreasing the number of the receivers may lead to a poorer spatial resolution of the surface elevation and higher ambiguity.

In the calculations reported in this section the 1-D rough surface $\zeta(x)$ was simulated with the Fourier series containing random phase and amplitudes assigned in accordance with the typical characteristics of gravity-capillary waves [12]. This gives

$$\zeta(x) = \sigma \sum_n C_n \cos\left(K_n x + \tau_n\right), \tag{26}$$

where σ is the standard deviation of the rough surface elevation (mean roughness height), K_n is wavenumber in the surface roughness spatial spectrum, τ_n is phase which value is randomly generated and amplitude C_n is defined by the correlation function of the waves of which the surface roughness pattern is composed and it is proportional to the wavelength l_n of the n-th harmonic in the Fourier expansion so that

$$C_n \sim \left(\frac{2\pi}{l_n}\right)^{\alpha/2}. \tag{27}$$

In particular the amplitude of each term in the Fourier expansion is linked to the power spectrum slope defined by the power of $\alpha = -4$ [13]. The surface elevation constructed with this kind of spatial spectrum supported multiple scales ranging from 8 mm to 115 mm and satisfied the condition (2) on the validity of Kirchhoff approximation. The standard deviation of the surface is set to $\sigma = 1$ mm.

Figure 3(a) shows the surface elevation simulated with the Fourier series using the range of spatial wavelengths of 8mm $< l_n <$ 115 mm and compared with surface elevation reconstructed with the proposed inversion method. This figure also shows the absolute error in the surface reconstruction which was calculated as $\epsilon_\zeta(x) = |\zeta_p(x) - \zeta_s(x)|$, where $\zeta_p(x)$ is the surface elevation predicted with the inverse method and $\zeta_s(x)$ is the surface elevation simulated with equation (26). The inversion was applied to the surface interval containing $M = 3000$ surface points that included the specular reflection point and its vicinity. It can be seen from the data presented in Figure 3 that the range of x for which the surface roughness reconstruction could be

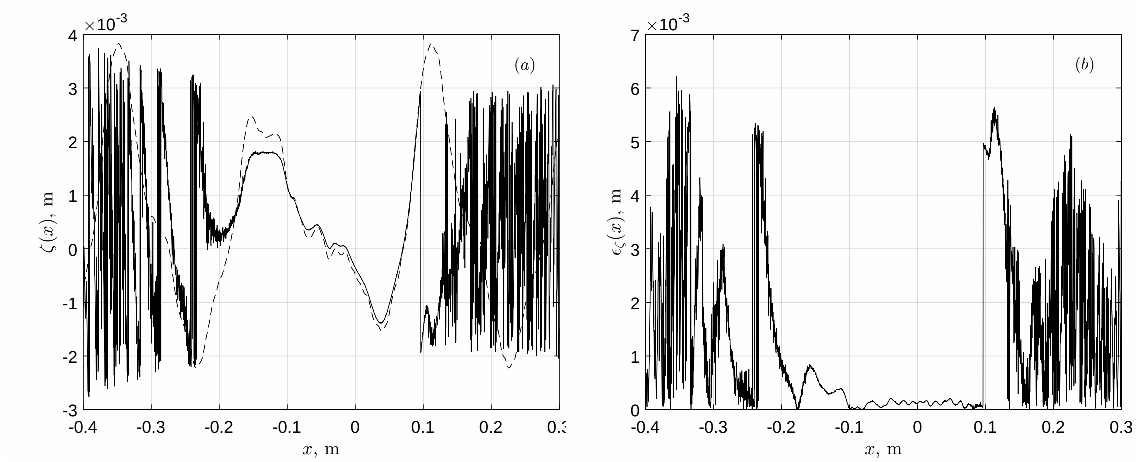

(a) (b)

Figure 3: (a) An example of the surface realization, $\zeta(x)$, (dashed line) used in equation (8) and its reconstruction from the Kirchhoff approximation (solid line) based on equation (23). (b) Absolute error of the reconstructed surface.

achieved was limited by the position of the specular reflection point which was in the range of -0.1 m $< x <$ 0.1 m. In particular, this is illustrated in Figure 3(b) where the absolute error of the surface reconstructed within this interval is limited and does not exceed 0.22 mm which is considerably smaller than the maximum roughness height of 2.5 mm. The root mean square (RMS) error for this range does not exceed 0.12 mm that is 12% of the true mean roughness height. In this analysis the root mean square error was calculated as

$$\epsilon_{\mathrm{rms}} = \sqrt{\frac{1}{N}\sum_{n=1}^{N}[\zeta_p(x_n) - \zeta_s(x_n)]^2}, \tag{28}$$

where the deduced surface elevation $\zeta_p(x_n)$ and simulated surface elevation $\zeta_s(x_n)$ are taken at the point x_n. It is noted that these errors are comparable or smaller to those which are typical for an alternative laser-induced fluorescence (LIF) method

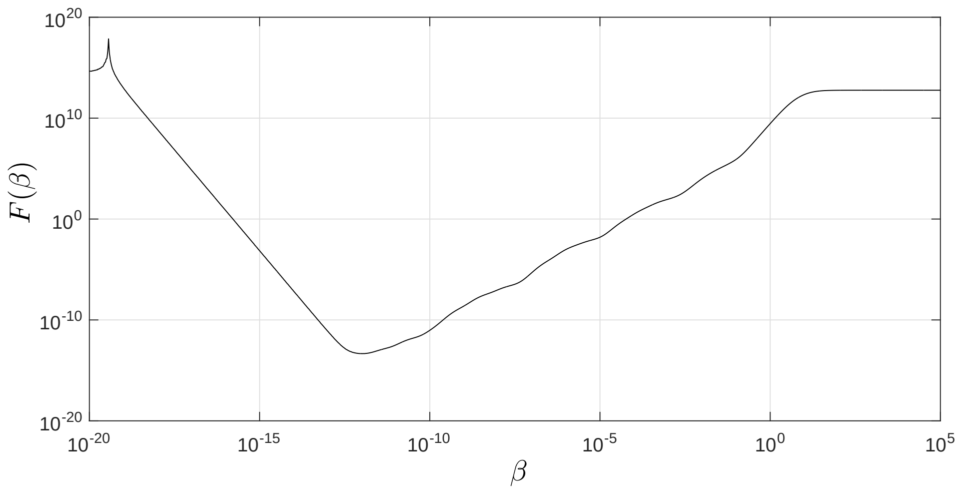

Figure 4: An example of the behaviour of the function $F(\beta)$ for the range of $10^{-20} < \beta < 10^{5}$.

(e.g. ± 0.14 mm for the LIF method used in ref. [10]).

The regularization parameter β was selected in accordance with equation (19). Figure 4 illustrates the variation of the GCV function F for the reconstruction process for the surface shown in Figure 3(a). The parameter β is small ($\beta \sim 10^{-12}$) and defines the threshold below which equation (18) becomes unstable. It increases with the decrease in the number of receivers causing the inversion process to become more unstable.

In order to understand the range of scales which can be recovered with equation (18) we compared the power spectrum of the surface roughness for a representative number of realizations obtained by varying randomly phase with the amplitudes of the Fourier expansion (equation (26)). The power spectrum was calculated by applying the Hanning window and Fourier transform to the original and recovered surface elevation data for each of the surface realization. It was then averaged over all the surface realizations. It was found that the average power spectrum converges

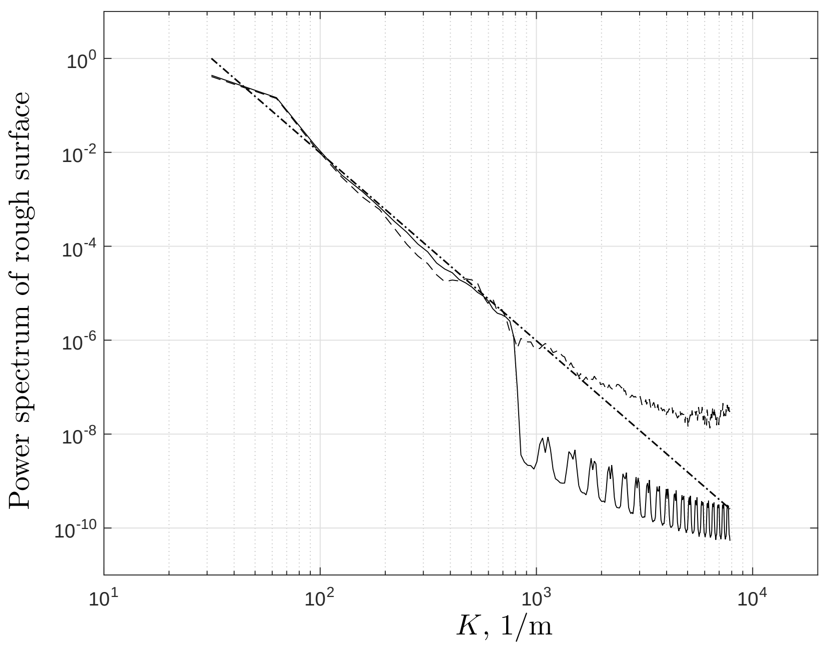

Figure 5: The normalized power spectrum averaged over 100 surface elevation realizations. Dash-dot line - the spectrum based on equation (27); dashed line - the inverted spectrum; solid line - the spectrum of the surfaces generated with equation (26).

to the true mean value to within 1% provided that at least 100 surface realizations were used. The average power spectrum inverted with the proposed method follows the slope $\alpha = -4$ defined by equation (27) for $K < 800$ 1/m (Figure 5). This corresponds to the lowest scale present in the simulated surface roughness wavelength of $l_n \approx 8$ mm. For the spectrum of larger scales (centimetre scale) when $K < 800$ the agreement between the average spectrum inverted with the proposed technique and that defined by equation (26) was within 15%.

B Measured roughness

In order to illustrate the application of the inversion method developed in Section III we used the acoustic pressure data $\boldsymbol{P}_{N\times 1}$ calculated with the Kirchhoff approximation and with the full-wave 2-D FDTD method [14] for a range of roughness realizations measured with the light-induced fluorescence method detailed in [10]. In the case of the Kirchhoff approximation the acoustic pressure was calculated as described in the previous section.

In the case of the FDTD method the acoustic pressure was computed for a source with directivity pattern defined by (25). This source directivity was simulated by setting up a 33 mm long line array of 49 point sources operated in phase. The frequency of the acoustic wave emitted by the source was $f = 43$ kHz. The time and space discretization intervals in the FDTD calculations were 1.03 μs and 0.5 mm, respectively [15].

The surface roughness data used in this work were obtained in a hydraulic flume with the method detailed in [10] and these were assumed to be exact in our calculations. The flume had a bed of hexagonally packed spheres with a diameter of 25 mm, and was tilted to a slope of $S_0 = 0.004$. The flow was turbulent, uniform and constant velocity was maintained across the length of the measured spatial interval. The surface elevation data was collected for four flow regimes which corresponded to the flow with the 60, 70, 80 and 90 mm of uniform water depth, respectively. These regimes corresponded to the mean flow velocity of 0.43, 0.50, 0.57 and 0.65 m/s, respectively. The arrangement of the receiver positions in the models was identical to that detailed in the previous section for a given realization of $\zeta(x)$.

In Figure 6 the real and imaginary parts of the angular dependent acoustic pressure predicted with the FDTD method is compared against that predicted with the

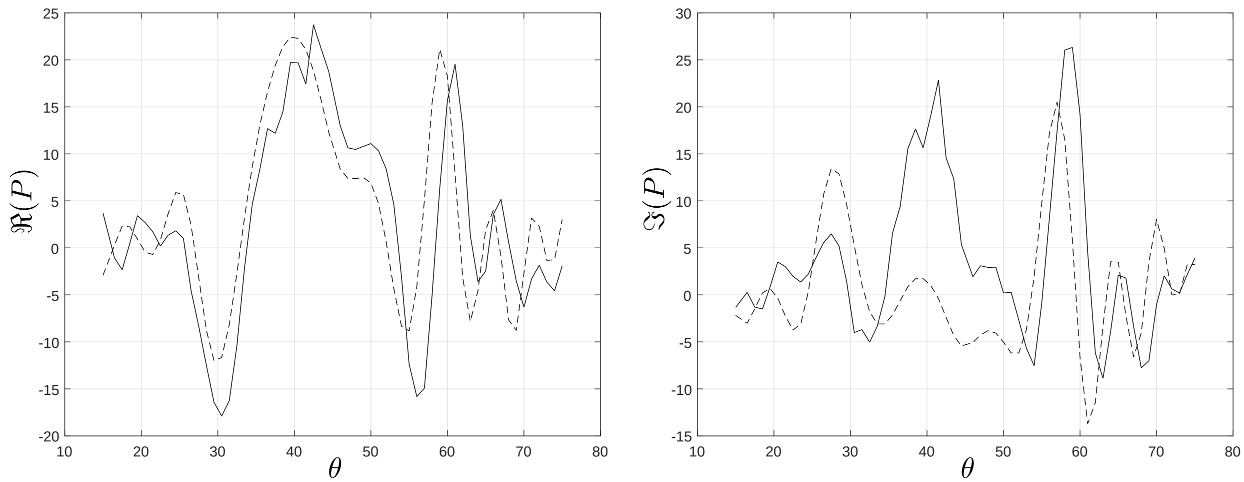

(a) (b)

Figure 6: The scattered acoustic pressure for a single realization of the rough surface elevation for flow depth 60 mm predicted with FDTD method(solid line) and Kirchhoff approximation (8) (dashed line). (a) Real part, (b) imaginary part.

Kirchhoff approximation (8). These results correspond to a realistic flow surface roughness realization measured for the 60 mm deep flow regime. The results suggest that the Kirchhoff approximation generally underpredicts the acoustic pressure in comparison to that predicted by the FDTD method. This is particularly noticeable in the case of the imaginary part and for the angles of incidence close to 45^o. These acoustic pressure data were then used with the proposed inversion technique to reconstruct the flow surface roughness.

Figures 7 (a)-(d) present the results of the application of the inverse technique to the acoustic pressure data predicted with the Kirchhoff approximation and with the FDTD method for flow surface realizations representing each of the four flow regimes. The inversion results are shown in the range $-0.1 < x < 0.1$ m where the maximum relative error was within 45% when the acoustic pressure was predicted with the FDTD method and 20% when the acoustic pressure was predicted with the Kirchhoff approximation. Within this interval the effects of shadowing and multiple scattering are relatively small that enables us to use equation (8) as an accurate approximation to the full-wave FDTD results. In all cases the minimum of β was in the interval $[0, 1]$ and its values is listed in Table 1. The accuracy we achieved depended on how far the point on the surface was from the nominal specular reflection point.

Figure 8 presents the mean spatial spectra which demonstrate the range of scales of roughness which were recovered through the proposed inversion technique. These spectra were inverted using the acoustic pressure data predicted with the Kirchhoff approximation and with the FDTD method. As it was noted in the previous section IV A, the normalized power spectrum provides information on the contribution of different roughness scales to the pattern of waves observed on the surface. For the four flow regimes considered in this work the recovered surface predicts the actual slope of the power spectrum closely for $K < 1000$ 1/m. However, it is clear that the accuracy of the proposed inversion techniques deteriorates as K approaches 1000 1/m that limits the use of the technique to identify the correct range of roughness scales, i.e. those scales which are at a $l_n < 6.3$ mm spatial wavelength. This can be explained by the limitations of the Kirchhoff approximation (equation (8)) as the local radius of curvature increases with the decrease of the surface scales. It is also noted that, although in this paper the coordinates of the receivers are exact, the implementation of the method can be limited by the uncertainties in the receiver positions. The sensitivity of the proposed method is analysed on Appendix A.

It is difficult to obtain a useful measure of the error between the measured spectrum and that reconstructed with the proposed inversion method by comparing these spectra directly. This is because the spectral power shown in Figure 8 varies by 10

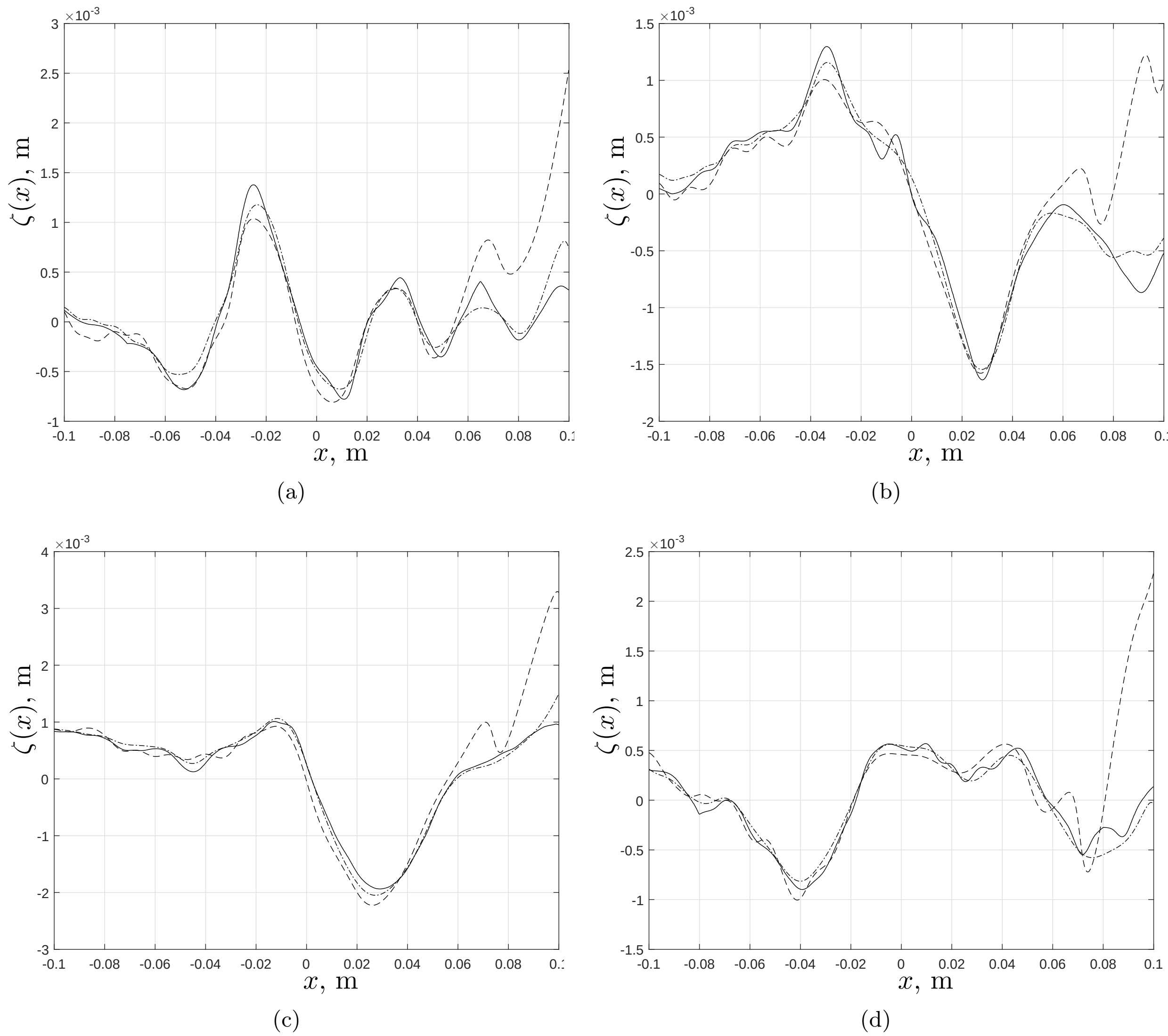

Figure 7: Examples of the surface elevation $\zeta(x)$ for the four flow regimes. Solid line - measured with the LIF method; dashed line - reconstructed with the sound pressure data predicted with the FDTD mode; dashed-dot line - reconstructed with the acoustic pressure data predicted with the Kirchhoff approximation. (a) Flow depth 60 mm, (b) flow depth 70 mm, (c) flow depth 80 mm, (d) flow depth 90 mm.

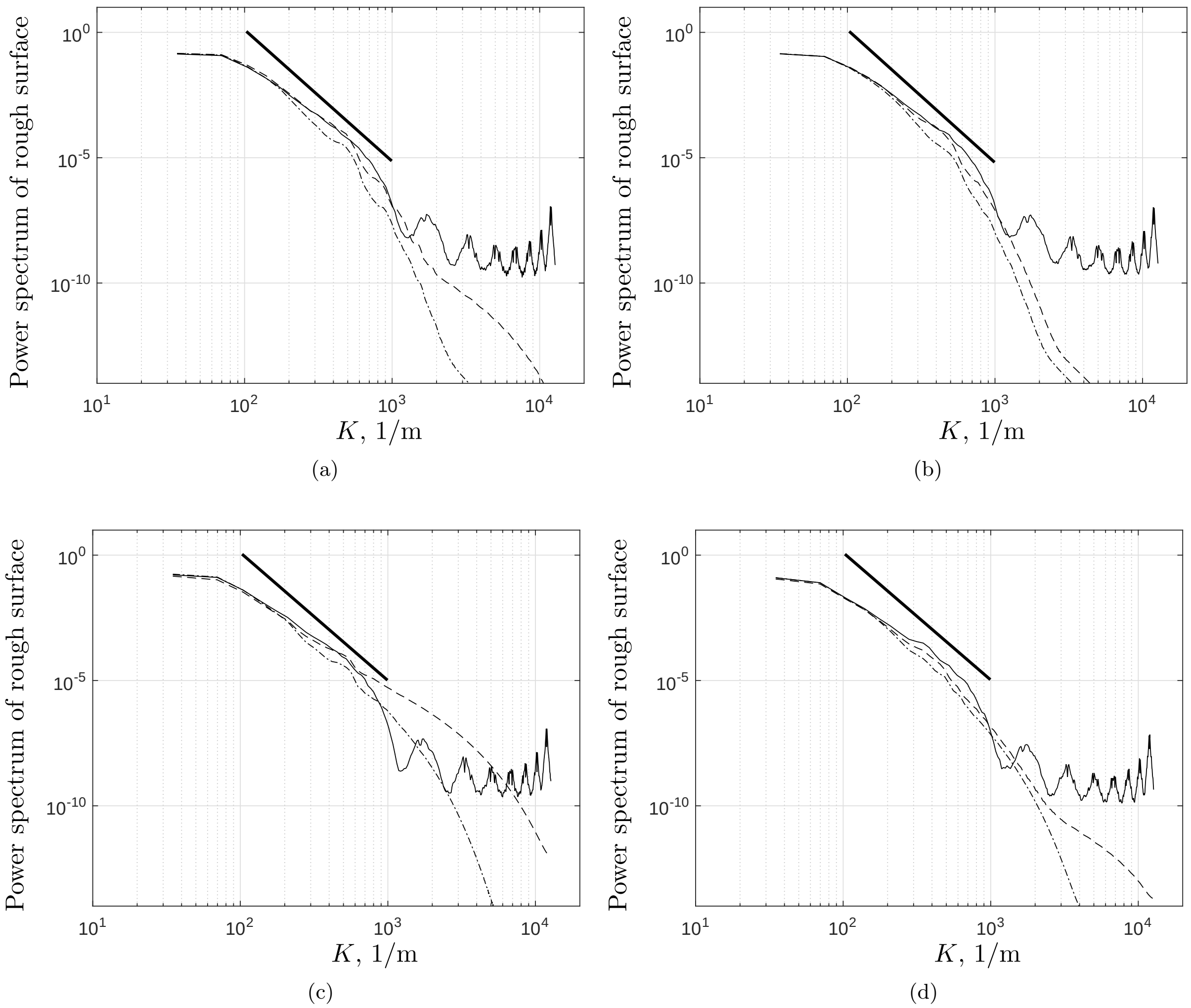

Figure 8: The normalized power spectrum of rough surface (solid line) compared against the power spectrum of the reconstructed surface where dashed and dashed-dot lines represent the use of FDTD and Kirchhoff approximation data, respectively. Thick solid line represents slope of the reconstructed power spectrum. (a) Flow depth 60 mm, (b) Flow depth 70 mm, (c) Flow depth 80 mm, (d) Flow depth 90 mm.

orders of magnitude over the considered range of wavenumbers. For this purpose all results in Figure 8 are compared against slope of the measured surface which is deduced with the linear regression technique between $K > 100$ and $K < 1000$ 1/m. The slope of the measured power spectrum for all flow regimes is approximated by $\alpha = -5$. A comparison between fitted line with slope -5 and spectra recovered with the proposed acoustic method suggests that the method provides adequate prediction of the surface power spectrum.

V Conclusion

In this paper we demonstrate the derivation of an inversion method based on the Kirchhoff approximation of the boundary integral equation and the application of an inverse technique based on SVD and Tikhonov regularization to an underdetermined system of equations. The surface roughness data we used in our work were simulated surface roughness and surface roughness measured with the LIF method that were assumed to be exact. The proposed inversion method enables us to determine the 1-D surface roughness with a maximum RMS error of 45% (FDTD method) and 20% (Kirchhoff approximation), both being sub-millimeter scale errors. This method also enables us to estimate the average spatial power spectrum of the surface roughness for the range of wavenumbers $K < 1000$ 1/m. This corresponds to spatial wavelengths of $l_n > 6.3$ mm. For the simulated surface roughness this spectrum converges to its true mean value to within 15% provided that at least 100 realizations are used in the averaging process. The area of the rough surface which can be reconstructed with the proposed acoustic setup and with the reported accuracy is within ± 0.1 m range. This range determines the maximum wavelength in the spatial spectrum of surface which can be estimated with the proposed acoustic setup and it is limited by the wavelength of the incident acoustic waves, by the number and arrangement of the receivers in the microphone array and by the adopted directivity of the sound source. It is shown that the reconstructed surface roughness power spectrum follow a power law characterising the simulated/measured surfaces.

The inversion method requires further improvements to increase accuracy for the scales in the centimeter and sub-centimeter range of spatial wavelength. This should involve the use of an extension of Kirchhoff approximation which can account for higher roughness slopes or a more refined 3D numerical model for 2D roughness. The retrieved roughness profiles can be used to find key statistical and spectral characteristics of the water surface. The proposed method can potentially be used together with the acoustic array measurements to accurately retrieve the temporal and spatial profile of the dynamic shallow water flow.

Acknowledgments

The authors are grateful to Dr. Andrew Nichols (University of Sheffield) for the provision of the LIF data some of which we used for the analysis reported in Section IV B. The authors would like to thank unanimous reviewer of this paper for valuable comments and suggestions.

Appendix A: Sensitivity

In order to test the sensitivity of the proposed inverse method it is necessary to simulate some type of geometrical uncertainty. In the case when position of all receivers are fixed the uncertainty in position is linked to the coordinates of the array frame. In this paper the frame is circular arch with radius $R = 0.4$ m. For

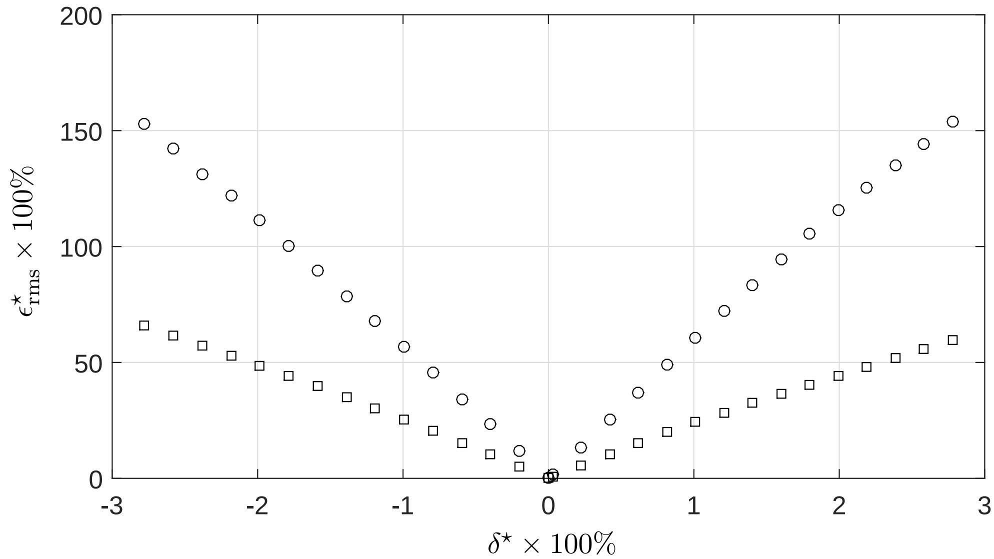

Figure 9: The relative variation in the RMS surface roughness height reconstructed for a given uncertainty in the x (squares) and z-coordinates (circles) for the receiver position

the 1D surface roughness the coordinates of the array frame can be varied along Oz and Ox axis. Introducing a small perturbation $\delta = \delta^\star R$, where $\delta^\star$ is dimensionless small parameter, to the distances R_1 and R_2 shown in equations (6) and (7) the uncertainty along Ox axis can be defined by

$$R_1 = \sqrt{(x - x_1 + \delta)^2 + z_1^2}, \tag{29}$$

$$R_2 = \sqrt{(x - x_2 + \delta)^2 + z_2^2}. \tag{30}$$

whereas the uncertainty along Oz axis is given by

$$R_1 = \sqrt{(x - x_1)^2 + (z_1 + \delta)^2}, \tag{31}$$

$$R_2 = \sqrt{(x - x_2)^2 + (z_2 + \delta)^2}. \tag{32}$$

In both cases dimensionless parameter $\delta^\star$ varies within 3% of frame radius R around frame initial coordinates. The results are shown in Figure 9 where the uncertainty is introduced in the inversion with the FDTD simulation of acoustic scattering. It is observed that the variation along the Oz axis depicted in circles results in a higher relative deviation in the RMS roughness height defined by

$$\epsilon^\star_{\mathrm{rms}}(\delta^\star) = \frac{\sqrt{\sum_{n=1}^{N}[\zeta_p(x_n, \delta^\star) - \zeta_p(x_n, \delta^\star = 0)]^2}}{\sqrt{\sum_{n=1}^{N}[\zeta_p(x_n, \delta^\star = 0)]^2}}, \tag{33}$$

within which ζ_p represents the predicted surface roughness with the inverse method. The root mean square (RMS) roughness hight reconstructed in the $[-0.1, 0.1]$ m spatial interval deviates linearly from the predicted initial ($\delta = 0$) RMS roughness hight as the position of the frame varies within 3% from the initial position. The uncertainty in Ox coordinate of the frame $\delta^\star \times 100\% = \pm 1\%$ with respect to its radius R results in 25% variation in the RMS roughness height. Applying the same

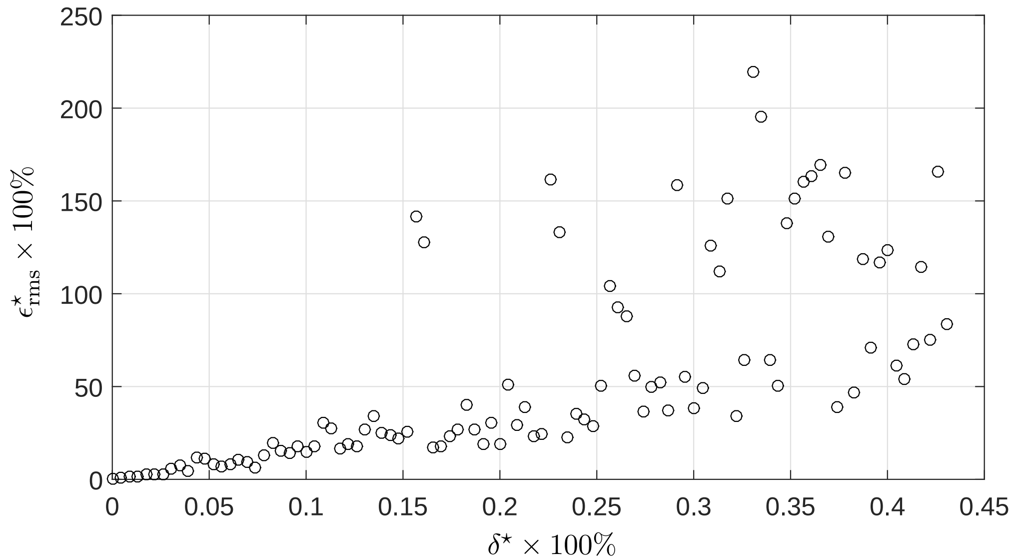

Figure 10: Relative variation in RMS surface roughness height computed for randomly perturbed positions of the receivers

uncertainty to the z coordinate of the receiver position results in approximately 50% deviation in the RMS roughness height from the initial solution.

To test the uncertainty in the receiver position it is proposed to introduce a random perturbation. The coordinates of all the 121 receivers are perturbed randomly with a uniform distribution in the circle which radius $\delta^\star$ does not exceed half of the distance between two adjacent receivers which is approximately 3 mm. The results are shown in Figure 10. It is suggested that increasing the radius of the perturbation results in a significant increase in the variation of the RMS roughness height calculated with equation (33). For 0.1% uncertainty in the position of each sensor the relative variation of the RMS roughness height is below 20% whereas at uncertainty approaching 0.5% (i.e. receiver is randomly positioned in the circle with radius approaching 1.5 mm) of frame radius R the relative variation $\epsilon^\star_{\text{rms}} \times 100\%$ is above 50%

that makes the inverse method invalid for reconstruction of roughness in the given spatial interval. It is clear that method is 10 times more sensitive to the uncertainty in the individual position of each receiver in the array compared to the uncertainty in the position of the whole array.

References

[1] R.J. Wombell and J.A. DeSanto, "The reconstruction of shallow rough-surface profiles from scattered field data," Inverse Problems, 7, 7–12 (1991).

[2] S.P. Walstead and G.B. Deane, "Reconstructing surface wave profiles from reflected acoustic pulses," J. Acoust. Soc. Am., 133, 2597–2611 (2013).

[3] K. V. Horoshenkov, A. Nichols, S. J. Tait, G. A. Maximov, The pattern of surface waves in a shallow free surface flow, J. Geoph. Res., 118, 1864-1876 (2013).

[4] A. Krynkin, K. V. Horoshenkov, A. Nichols and S. J. Tait, "A non-invasive acoustical method to measure the mean roughness height of the free surface of a turbulent shallow water flow," Review of Scientific Instruments, 85 (11), 114902, (2014).

[5] A. Ishimaru, *Wave Propagation and Scattering in Random Media* (Academic Press, Inc., New York, 1978), pp. 484–487.

[6] E.I. Thorsos, "The validity of the Kirchhoff approximation for rough surface scattering using a Gaussian roughness spectrum," J. Acoust. Soc. Am., 83, 78–92 (1988).

[7] F. G. Bass and I. M Fuks, *Wave Scattering from Statistically Rough Surfaces* (Pergamon Press, Ltd, Oxford, 1979), p. 228.

[8] W. H. Press, S. A. Teukolsky, W. T. Vetterling and B. P. Flannery, *Numerical Recipes: The Art of Scientific Computing* (3rd Edition, Cambridge University Press, Cambridge, 2007), pp. 65–75.

[9] H.W. Engl, M. Hanke and A. Neubauer, *Regularization of Inverse Problems*, (Kluwer Academic Publ., Dordrecht, 2000), pp. 221–237.

[10] A. Nichols, *The Interaction Mechanism of Airborne Acoustic Fields with Turbulent Shallow Flows* (Ph.D. thesis, University of Bradford, UK, 2014), pp. 76–79.

[11] Q. Leclére, "Acoustic imaging using under-determined inverse approaches: Frequency limitations and optimal regularization", J. Sound Vib., 321, 605–619, (2009).

[12] J.A. Toporkov and G.S. Brown, "Numerical Simulations of Scattering from Time-Varying, Randomly Rough Surfaces", IEEE T. Geosci. Remote, 38, 1616–1625 (2000).

[13] O. M. Phillips, "On the generation of waves by turbulent wind," J. Fluid Mech., 2, 417–445 (1957).

[14] T. Van Renterghem, "Efficient outdoor sound propagation modeling with the finite-difference time-domain (FDTD) method: a review," Int. J. Aeroacoustics, 13 (5-6), 385–404 (2014).

[15] K. V. Horoshenkov, T. Van Renterghem, A. Nichols and A. Krynkin, "Finite difference time domain modelling of sound scattering by the dynamically rough surface of a turbulent open channel flow," Applied Acoustics, 110, 13–22 (2016)

Table 1: Examples of the minimum values of the regularization parameter β obtained for 4 realizations of the surface elevation associated with the four adopted flow regimes.

	60 mm	70 mm	80 mm	90 mm
$\beta \times 10^7$	8.4	8.4	8.4	13

.

List of Figures